THE JOURNAL OF PHYSICAL CHEMISTRY Letters

Letter

pubs.acs.org/JPCL

Computational Design of a Family of Light-Driven Rotary Molecular Motors with Improved Quantum Efficiency

Alexander Nikiforov,[†] Jose A. Gamez,[‡] Walter Thiel,[†] and Michael Filatov*[,¶,§]

[†]Max-Planck-Institut für Kohlenforschung, Kaiser-Wilhelm-Platz 1, D-45470 Mülheim an der Ruhr, Germany

[‡]Institute of Technical and Macromolecular Chemistry, RWTH Aachen University, Worringerweg 1, 52074 Aachen, Germany

[¶]Department of Chemistry, Southern Methodist University, 3215 Daniel Avenue, Dallas, Texas 75275-0314, United States

[§]Department of Chemistry, School of Natural Sciences, Ulsan National Institute of Science and Technology (UNIST), Ulsan 689-798, Korea

Supporting Information

ABSTRACT: Two new light-driven molecular rotary motors based on the *N*-alkylated indanylidene benzopyrrole frameworks are proposed and studied using quantum chemical calculations and nonadiabatic molecular dynamics simulations. These new motors perform pure axial rotation, and the photochemical steps of the rotary cycle are dominated by the fast bond-length-alternation motion that enables ultrafast access to the S_1/S_0 intersection. The new motors are predicted to display a quantum efficiency higher than that of the currently available synthetic all-hydrocarbon motors. Remarkably, the quantum efficiency is not governed by the topography (peaked versus sloped) of the minimum-energy conical intersection, whereas the S_1 decay time depends on the topography as well as on the energy of the intersection relative to the S_1 minimum. It is the axial chirality (helicity), rather than the point chirality, that controls the sense of rotation of the motor.

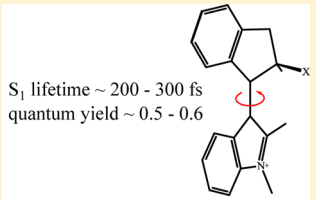

Design improves performance

Conversion of the energy of light to directional mechanical motion is one of the promising routes to building nanomachines for biological and chemical application.[1−3] Light-driven molecular rotary motors (molecular motors, in the following) utilize the photoinduced *cis*−*trans* (or *E*−*Z*) isomerization of the double bond (to date, C═C[4−7] and C═N[8]) to create a unidirectional rotary motion of the rotor part with respect to the stator part of the molecule. So far, the design of these motors was driven by empirical observation[7,9,10] and by attempts to mimic the naturally occurring light-driven molecular systems.[11] However, further improvement of their operational efficiency and the design of new classes of motors require rational rules which identify potentially useful types of molecules and relate their molecular structure to their functionality.[12,13]

In the ground (S_0) electronic state of the molecule, the double bond is sufficiently stiff to attain a nearly planar conformation, even when there is a substantial steric repulsion between substituent moieties. Photoexcitation of the double bond breaks its π-component and releases the strain energy by torsion (through ca. 90°) about the bond axis.[14] Introducing a chiral center near the isomerizing bond can break the symmetry between the clockwise (CW) and counterclockwise (CCW) rotation and lend the molecule the ability to perform a unidirectional rotation.[13] Reestablishing the double bond and resetting the molecule to a conformation suitable for further photoisomerization (at ca. 180° torsion) usually involves a thermally activated step, which results in a 4-stroke mechanism of motor operation.[4−7] Until now the thermally activated steps were the focus of synthetic work, e.g., aiming at modifications to increase the speed of rotation,[4−7] while the photoisomerization steps remained less amenable to chemical modulation.[10]

By contrast, a recently proposed new design principle[12] addresses the photoisomerization steps: the chemical modulation of the moieties at the isomerizing double bond to achieve energetic equalization between homolytic and heterolytic π-bond breaking. This should lead to the occurrence of S_0/S_1 conical intersections (CIs) at molecular geometries reached by torsion−bond length alternation (tor−BLA) distortions, while torsion−pyramidalization (tor−pyr) distortions are required for molecules in which the homolytic π-bond breaking is energetically preferred.[12,14,15] Because the CIs are the (manifolds of) points at which the $S_1 \rightarrow S_0$ nonadiabatic population transfer occurs,[16] their conformation is important for the sequence of geometric transformations during photoisomerization. For example, in all-hydrocarbon motors, e.g., motors based on sterically overcrowded alkene frameworks,[4−7] a substantial pyramidalization is needed alongside the torsion to reach the CI region.[17−19] This results in a hippopede (or lemniscate) type of motion which strongly deviates from the desired axial rotation.[12,17,18] Replacing tor−pyr CIs by tor−BLA CIs will favor pure axial rotation and should result in a higher quantum efficiency of the motor.[12]

Here, we test the proposed design principle[12] by computationally investigating the dynamics of a new class of molecular motors constructed accordingly. The new motors, collectively

Received: November 18, 2015
Accepted: December 15, 2015
Published: December 15, 2015

DOI: 10.1021/acs.jpclett.5b02575
J. Phys. Chem. Lett. 2016, 7, 105−110

designated as NAIBP (*N*-alkylated indanylidene benzopyrrole) motors (see Scheme 1), are closely related to molecular

Scheme 1. Chemical Formula and Atomic Numbering of NAIBP Motors Studied in This Work[a]

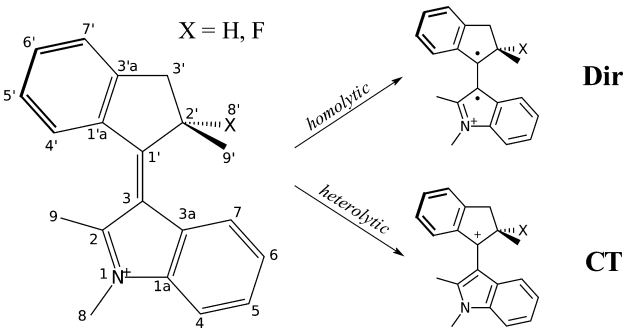

[a]Also shown are the Lewis structures corresponding to the homolytic (diradicaloid, Dir) and heterolytic (charge transfer, CT) breaking of the $C_3{=}C_{1'}$ π-bond.

switches that are inspired by the retinal chromophore and utilize protonated Schiff bases in their design.[20−22] Compared with these molecular switches, the NAIBP molecular motors contain an extra benzene ring which results in an increased steric strain and a pronounced helicity of the ground-state conformations; specifically, we study 3-[(2R)-2-methyl-1-indanylidene]-1-methyl-2-methylindole (H-NAIBP) and 3-[(2S)-2-fluoro-2-methyl-1-indanylidene]-1-methyl-2-methylindole (F-NAIBP). Unlike the achiral switches, the NAIBP motors feature a chiral center at the 2′ position (see Scheme 1). In the S_0 state, the NAIBP motors exist as *E* or *Z* conformers with P or M helicity, i.e. in *EP*, *EM*, *ZP*, and *ZM* conformations. In the following, we classify these conformations by assuming that the substituent X is always of higher priority, and we consider only the *R* enantiomer of H-NAIBP and the *S* enantiomer of F-NAIBP.

An analysis of the NAIBP motors using the fragment approach[12] shows that heterolytic π-bond breaking (leading to species with charge transfer (CT) character, see Scheme 1) is favored over homolytic π-bond breaking (leading to diradicaloid species) by 22 and 11 kcal/mol for H-NAIBP and F-NAIBP, respectively. Hence, along the π-bond torsion coordinate, the S_0 state acquires CT character, while the S_1 state becomes diradicaloid (see also the Supporting Information).[14] Thus, the S_1/S_0 crossing at ca. 90° of indanylidene torsion is accompanied by a BLA distortion,[12] which together with the torsion spans the so-called branching plane (BP) that collects the displacements lifting the S_1/S_0 degeneracy at the CI.[16] Hence, the new motors should possess CIs of tor−BLA type, perform a nearly axial rotational motion upon photoexcitation, and show a high photoisomerization quantum yield.

Here, we test this conjecture by performing static calculations on the S_1 and S_0 potential energy surfaces (PESs) at the DFT REKS level[23,24] and the semiempirical OM2/MRCI level[25−27] (see the Supporting Information for details) and by studying the photoisomerization dynamics through OM2/MRCI-based trajectory surface hopping (TSH) nonadiabatic molecular dynamics (NAMD) simulations.[28−32] Based on the topography of the S_0 and S_1 PESs, the working cycle of the NAIBP motors is a 4-stroke sequence shown in Scheme 2, with two photoisomerization steps and two thermally activated helix inversion steps that lead to an overall CCW rotational motion

Scheme 2. Schematic Representation of the Working Cycle of NAIBP Motors

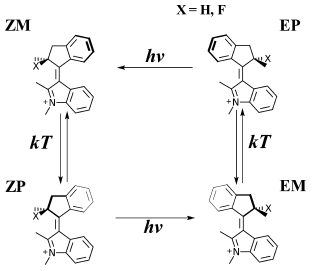

of the indanylidene moiety; in Scheme 2 it is assumed that only the P helical conformers are photoexcited at the beginning of each photoisomerization step.

Figure 1 shows the UV/vis absorption spectra of the ground-state conformers of the two NAIBP motors obtained at their

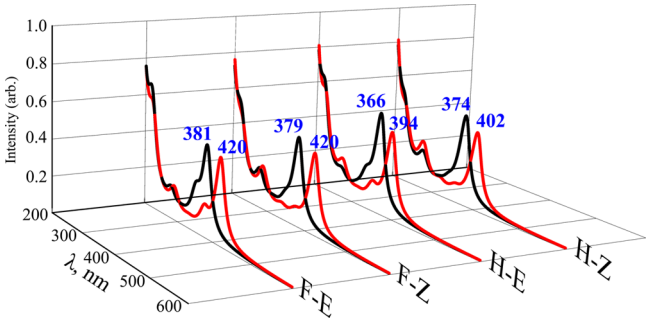

Figure 1. Theoretical UV/vis absorption spectra of the NAIBP motors studied in this work. The spectra are constructed from TD-BH&HLYP/6-31G* excitation energies and intensities using Lorentz broadening with half-width at half-maximum of 15 nm. Color code: black (red) lines, spectra of the conformers with P (M) helicity.

equilibrium geometries (see the Supporting Information) from TD-BH&HLYP/6-31G* calculations.[33−37] The first absorption maxima of the P and M forms are separated by a wavelength gap of ca. 30−40 nm such that irradiation at $\lambda \approx 365{-}380$ (410−420) nm should excite the P (M) helical form with sufficient selectivity. This satisfies one of the basic prerequisites for the validity of the working cycle shown in Scheme 2. Provided that each helical form photoisomerizes predominantly in one possible direction (e.g., P form in the CCW and M form in the CW sense), irradiation with light of suitable wavelength can be used to control the sense of rotation of these motors.

The S_1 state of the NAIBP motors, irrespective of the substituent X, corresponds to a one-electron $\pi \rightarrow \pi^*$ transition localized mostly on the $C_3{=}C_{1'}$ bond. It is optically bright (oscillator strength $f \approx 0.4$). Figure 2 shows the S_0 and S_1 potential energy profiles along a reaction coordinate representing the indanylidene torsion. In the S_0 state the barriers to $C_3{=}C_{1'}$ π-bond torsion are sufficiently high so that *E*/*Z* interconversion should not occur thermally at ambient temperatures. The P and M helical forms of the *E* and *Z* conformers are separated by lower barriers in the range of 6−12 kcal/mol (Figure 2), implying a rather fast equilibration between these forms at ambient temperatures and even below. The P conformers of F-NAIBP are slightly favored over the M conformers, while both helical forms are nearly isoenergetic in H-NAIBP. The computed difference in the excitation energies of the P and M conformers ensures that

DOI: 10.1021/acs.jpclett.5b02575
J. Phys. Chem. Lett. 2016, 7, 105−110

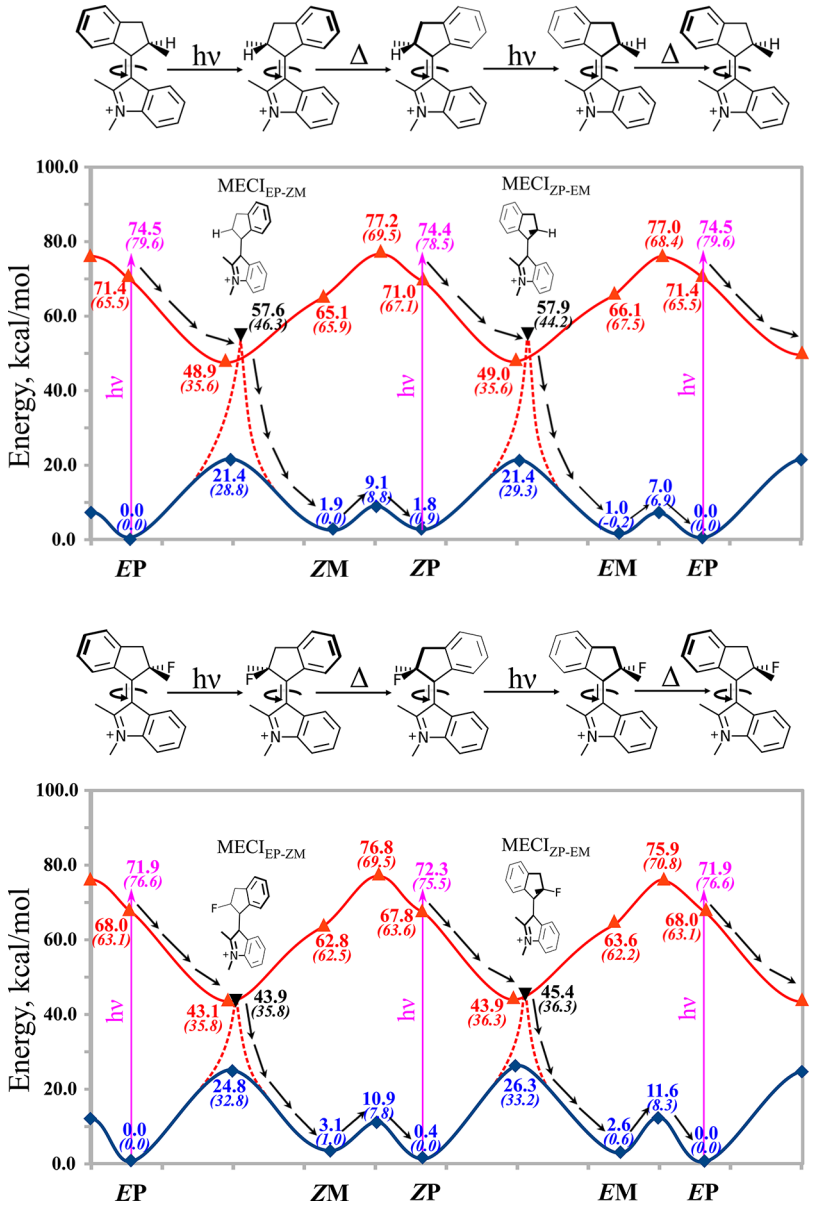

Figure 2. Schematic representation of the potential energy profile of the S_0 (blue) and S_1 (red) states of H-NAIBP (upper panel) and F-NAIBP (lower panel) along the torsional reaction coordinate, as obtained from SSR-BH&HLYP/6-31G* (numbers outside parentheses) and OM2/MRCI (in parentheses) calculations. The S_0 energy profile is constructed from the energies of the local minima and transition states optimized in the ground electronic state. The S_1 energy profile is obtained from the relaxed 2D PES scan of the lowest excited electronic state. The vertical arrows (magenta) show the vertical excitation energies at the Franck−Condon points.

only one form (P in Figure 2) is photoexcited when using a sufficiently narrow range of irradiation wavelengths.

The S_1 states of both motors have deep minima (ca. 30 kcal/mol) at the positions of the transition states for the S_0 E/Z isomerizations. In these minima, the $C_3{=}C_{1'}$ π-bond is broken; the corresponding torsion angle of the indanylidene moiety is ca. 90°. There are no barriers between the Franck−Condon (FC) points and these minima; therefore, an unobstructed torsional motion is possible in the S_1 state. The S_1/S_0 CIs are located near the S_1 minima (see Figure 2). The MECIs of the NAIBP motors are typical tor−BLA CIs (see the Supporting Information). They can be reached from the respective S_1 minima by a BLA distortion within the six-atom fragment shown in Figure 3. The $C_3{=}C_{1'}$ bond torsion and the BLA distortion lead away from the S_0/S_1 CI, and it is thus these modes that are involved in the population transfer during the photodynamics. The most significant difference between the two motors is the position of the MECIs on the energy scale: in F-NAIBP they are very close to the respective S_1 minima

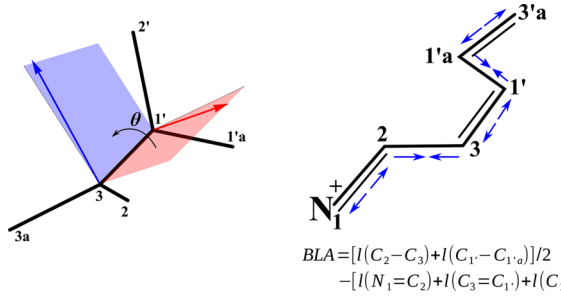

$$BLA = [l(C_2{-}C_3) + l(C_{1'}{-}C_{1'a})]/2 - [l(N_1{=}C_2) + l(C_3{=}C_{1'}) + l(C_{1'a}{=}C_{3'a})]/3$$

Figure 3. Definition of the dihedral angle, θ, and the BLA parameter.

DOI: 10.1021/acs.jpclett.5b02575
J. Phys. Chem. Lett. 2016, 7, 105−110

Table 1. Lifetimes of the S_1 State (τ, fs), Quantum Yields (ϕ) of Photoisomerization, and Photostationary State (PSS) Ratios for the Individual Steps of the Working Cycle of NAIBP Molecular Motors Obtained from OM2/MRCI NAMD Simulations

	H-NAIBP				F-NAIBP			
	EP → ZM	ZM → EP	ZP → EM	EM → ZP	EP → ZM	ZM → EP	ZP → EM	EM → ZP
τ_1	206	140	232	103	298	144	291	137
%	95	78	95	68	100	100	100	100
τ_2	284	375	316	405	–	–	–	–
%	5	22	5	33	–	–	–	–
ϕ	0.67	0.57	0.61	0.61	0.47	0.43	0.43	0.39
PSS(365)[a]	5.79		2.36		3.70		2.48	
PSS(410)	0.25		0.37		0.41		0.30	

[a]The PSS ratio includes the ratio of theoretically calculated absorptivities of the respective conformers (see Figure 1) at the specified wavelength λ (see text).

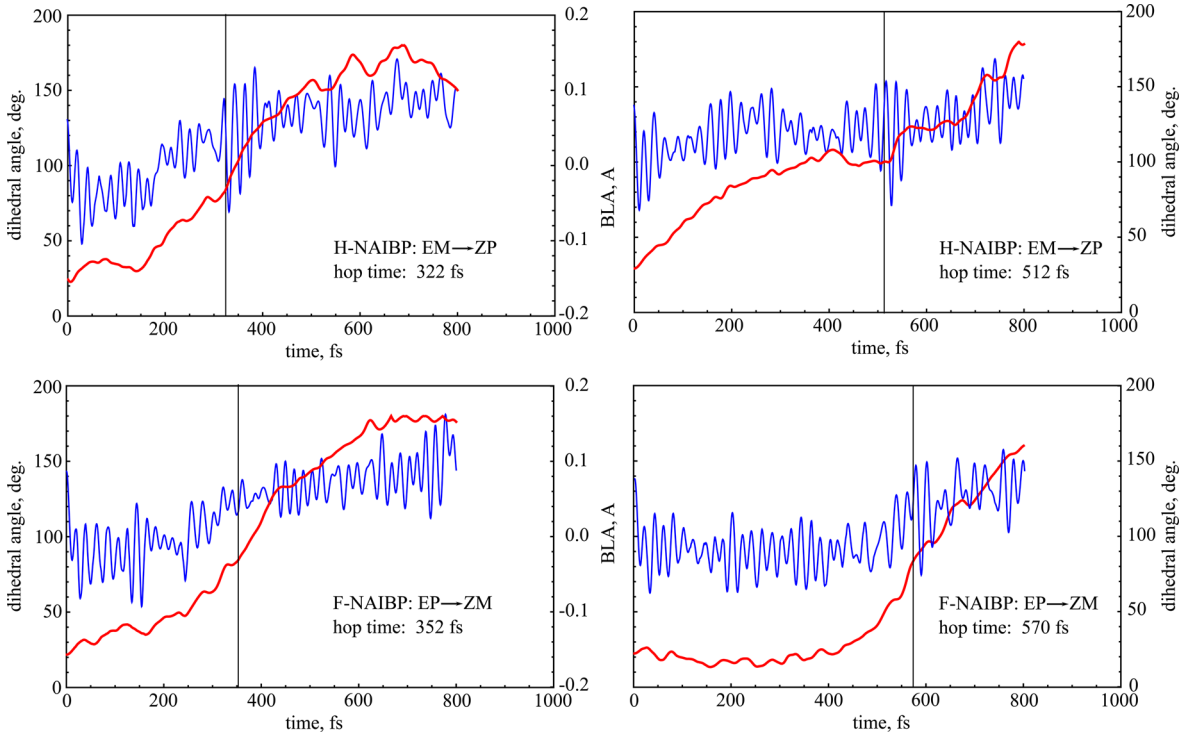

Figure 4. Evolution of the dihedral angle θ (red, see Figure 3 for definition) and BLA displacement parameter (blue) along typical nonadiabatic trajectories of H-NAIBP (upper panel) and F-NAIBP (lower panel). The chosen trajectories exemplify the observed fast (left) and slow (right) decay, see text.

(within ca. 1 kcal/mol or less), whereas they lie significantly above these minima in H-NAIBP (by ca. 9−10 kcal/mol). Topologically, the MECIs are thus nearly peaked in F-NAIBP and clearly sloped in H-NAIBP.

The TSH-NAMD simulations of the photodynamics of the two NAIBP motors (see the Supporting Information for the computational details) were carried out using only the OM2/MRCI method,[30−32] because NAMD simulations with the SSR method are not yet feasible. The use of OM2/MRCI is justified by the reasonably good agreement between the OM2/MRCI and SSR-BH&HLYP/6-31G*results for the S_0 and S_1 potential energy profiles (see above). Table 1 collects the S_1 state lifetimes, τ, and quantum yields, ϕ, of both motors averaged over more that 300 TSH-NAMD trajectories for each photoisomerization.

Generally speaking, both motors display ultrafast S_1 state dynamics ($\tau \approx 200$ fs). In both cases, the initial evolution along the trajectories starting from the FC points features a very rapid stretching of the $C_3{=}C_{1'}$ bond (ca. 10−15 fs) accompanied by an inversion of the lengths of the single and double bonds between the neighboring atoms. The sudden drop of the BLA parameter characterizing this distortion is clearly visible in Figure 4.

As shown in Figure 4, the BLA parameter (see Figure 3) experiences ultrafast quasiperiodic oscillations on the time scale of ca. 30 fs. The torsional motion proceeds on a much slower time scale and, in the range of $\theta \approx 90°$, the rapid BLA oscillations facilitate the approach to the CI seam. This picture of the dynamics in NAIBPs is markedly different from that in the all-hydrocarbon fluorene molecular motor.[17,18] The latter has tor−pyr CIs, and the reaction coordinate is spanned by the slow torsion and pyramidalization motions (time scale, ca. 1 ps). Thus, the CI can be easily missed if these motions do not rapidly adjust themselves to suitable values when the momentum is in the proper direction toward isomerization products.[17] This may be the reason behind the fairly low

DOI: 10.1021/acs.jpclett.5b02575
J. Phys. Chem. Lett. 2016, 7, 105−110

theoretical quantum efficiency of the fluorene motor ($\phi \approx 0.2-0.3$) and the rather long S_1 decay time (ca. 1.4 ps).[18] For NAIBPs, the situation is radically different because the CI seam is reached quickly owing to the rapid adjustment of the BLA distortion, and the quantum yield of isomerization is nearly doubled ($\phi \approx 0.5-0.6$, see Table 1).

While both NAIBP motors display ultrafast dynamics, it is only H-NAIBP that exhibits a biexponential decay, with discernible fast (ca. 100−200 fs) and slow (ca. 300−400 fs) components (see Table 1 and the Supporting Information). As can be seen in the upper panels of Figure 4, the fast S_1 trajectories of H-NAIBP (upper left) rapidly reach the CI region where they hop to the S_0 surface, while the slow trajectories (upper right) remain within the range of $\theta \approx 90°$ for about 200 fs or longer. Visual inspection of the geometries along these slow trajectories (see the media files in the Supporting Information) reveals that, instead of reaching the CI seam, H-NAIBP is trapped for 200−400 fs inside the S_1 minimum. For F-NAIBP, the CI is energetically very close to the S_1 minimum (see above); hence, no such "trapping" of trajectories is observed. The fast and slow S_1 trajectories in F-NAIBP differ mainly in the time that it takes initially to get away from the FC region, see lower panels of Figure 4. Hence, the dynamics of the two motors suggests that the topography of the S_1 PES and the positioning of the CI with respect to the S_1 minimum affects the lifetimes (fast/slow) and the character (monoexponential/biexponential) of the S_1 decay but not the quantum yield, which is found to be very high for both motors.

The photostationary state (PSS) ratios of the *EP* ⇄ *ZM* and *ZP* ⇄ *EM* photoequilibria of NAIBPs, see Table 1, were estimated from the quantum yields, ϕ, of the individual photosteps and the theoretical absorptivities, ϵ, at λ = 365 nm and λ = 410 nm using the equation $\mathrm{PSS}[A \rightleftarrows B] = \frac{[B]}{[A]} = \frac{\phi_A}{\phi_B}\frac{\epsilon_A}{\epsilon_B}$. At λ = 365 nm, the photoequilibrium is strongly shifted to the right side, i.e., toward the *ZM* and *EM* conformers, whereas at 410 nm it is shifted to the left, toward the *EP* and *ZP* conformers. Hence, a CCW rotation of indanylidene occurs at λ = 365 nm as the result of the *EP* → *ZM* and *ZP* → *EM* isomerizations. At λ = 410 nm, the dominating photosteps are reversed to *ZM* → *EP* and *EM* → *ZP*, and the sense of the indanylidene rotation is reversed to CW. It should be emphasized that the S_1 NAMD trajectories of the P (M) helical forms are always found to propagate in the CCW (CW) sense. Thus, the direction of rotation of the motor is governed by the helicity (axial chirality) and not by the point chirality; the point chirality of H-NAIBP (S) differs from that of F-NAIBP (R), but the direction of rotation remains the same at a given irradiation wavelength λ.

In conclusion, the study of the PESs and the nonadiabatic dynamics of photoisomerization of the proposed molecular motors confirms the validity of the guiding principle[12] used in their design: isoenergetic homolytic and heterolytic π-bond breaking leads to a tor−BLA character of the CI seam and increases the quantum efficiency of photoisomerization of these motors (from $\phi \approx 0.2-0.3$ for an all-hydrocarbon motor[18] to $\phi \approx 0.4-0.6$). Moreover, the tor−BLA CI character of the NAIBP motors results in pure axial rotation and ultrafast photoisomerization, on the time scale of 200 fs.

The NAMD simulations suggest that, in contrast to previous suggestions,[14,16] the topography of the CI seam does not play a decisive role for the quantum efficiency of photoisomerization. Equally high efficiency was observed for both motors, H-NAIBP with distinctly sloped CIs and F-NAIBP with nearly peaked CIs. The topography of the S_1 PES and the position and energy of the CI relative to the S_1 minimum strongly influence the dynamics of the S_1 decay, which is monoexponential when the CI is close to the S_1 minimum (F-NAIBP) and biexponential when the CI seam is elevated above this minimum (H-NAIBP). This observation may help to rationalize the results of ultrafast optical measurements where biexponential (and even multiexponential) decay is often observed.

The present NAMD simulations confirm that the helicity has a strong influence on the direction of rotation,[32] more so than the point chirality of the motors, because the trajectories starting from the FC points with P (M) helicity are always found to propagate in the CCW (CW) sense. Hence, selectively exciting conformers with specific helicity (with the use of a tunable light source) can control the sense of rotation of molecular motors.

■ ASSOCIATED CONTENT

Supporting Information

The Supporting Information is available free of charge on the ACS Publications website at DOI: 10.1021/acs.jpclett.5b02575.

Computational details, Cartesian coordinates and pictorial representations of all relevant species, population analysis of the S_0 and S_1 species along the trajectories, S_1 and S_0 PES scans near the MECI points, plots of excited-state populations and quantum yields as functions of time, and descriptions of media files (PDF)
Media files (ZIP)

■ AUTHOR INFORMATION

Corresponding Author

*E-mail: mike.filatov@gmail.com.

Notes

The authors declare no competing financial interest.

■ ACKNOWLEDGMENTS

This work was supported by an ERC Advanced Grant to W.T. (OMSQC). At the beginning of this work M.F. was supported by the FP7/2007-2013 IEF Grant 326652.

■ REFERENCES

(1) Browne, W. R.; Feringa, B. L. Making Molecular Machines Work. *Nat. Nanotechnol.* **2006**, *1*, 25−35.
(2) Balzani, V.; Credi, A.; Venturi, M. Light Powered Molecular Machines. *Chem. Soc. Rev.* **2009**, *38*, 1542−1550.
(3) Coskun, A.; Banaszak, M.; Astumian, R. D.; Stoddart, J. F.; Grzybowski, B. A. Great Expectations: Can Artificial Molecular Machines Deliver on Their Promise? *Chem. Soc. Rev.* **2012**, *41*, 19−30.
(4) Koumura, N.; Zijlstra, R. W. J.; van Delden, R. A.; Harada, N.; Feringa, B. L. Light-Driven Monodirectional Molecular Rotor. *Nature* **1999**, *401*, 152−155.
(5) Koumura, N.; Geertsema, E. M.; van Gelder, M. B.; Meetsma, A.; Feringa, B. L. Second Generation Light-Driven Molecular Motors. Unidirectional Rotation Controlled by a Single Stereogenic Center with Near-Perfect Photoequilibria and Acceleration of the Speed of Rotation by Structural Modification. *J. Am. Chem. Soc.* **2002**, *124*, 5037−5051.
(6) Pijper, D.; van Delden, R. A.; Meetsma, A.; Feringa, B. L. Acceleration of a Nanomotor: Electronic Control of the Rotary Speed of a Light-Driven Molecular Rotor. *J. Am. Chem. Soc.* **2005**, *127*, 17612−17613.

DOI: 10.1021/acs.jpclett.5b02575
J. Phys. Chem. Lett. 2016, 7, 105−110

(7) Pollard, M. M.; Meetsma, A.; Feringa, B. L. A Redesign of Light-Driven Rotary Molecular Motor. *Org. Biomol. Chem.* **2008**, *6*, 507−512.
(8) Greb, L.; Lehn, J.-M. Light-Driven Molecular Motors: Imines as Four-Step or Two-Step Unidirectional Rotors. *J. Am. Chem. Soc.* **2014**, *136*, 13114−13117.
(9) Landaluce, T. F.; London, G.; Pollard, M. M.; Rudolf, P.; Feringa, B. L. Rotary Molecular Motors: A Large Increase in Speed through a Small Change in Design. *J. Org. Chem.* **2010**, *75*, 5323−5325.
(10) Conyard, J.; Cnossen, A.; Browne, W. R.; Feringa, B. L.; Meech, S. R. Chemically Optimizing Operational Efficiency of Molecular Rotary Motors. *J. Am. Chem. Soc.* **2014**, *136*, 9692−9700.
(11) Gozem, S.; Melaccio, F.; Luk, H. L.; Rinaldi, S.; Olivucci, M. Learning from Photobiology how to Design Molecular Devices Using a Computer. *Chem. Soc. Rev.* **2014**, *43*, 4019−4036.
(12) Filatov, M.; Olivucci, M. Designing Conical Intersections for Light-Driven Single Molecule Rotary Motors: From Precessional to Axial Motion. *J. Org. Chem.* **2014**, *79*, 3587−3600.
(13) Marchand, G.; Eng, J.; Schapiro, I.; Valentini, A.; Frutos, L. M.; Pieri, E.; Olivucci, M.; Léonard, J.; Gindensperger, E. Directionality of Double-Bond Photoisomerization Dynamics Induced by a Single Stereogenic Center. *J. Phys. Chem. Lett.* **2015**, *6*, 599−604.
(14) Bonačić-Koutecký, V.; Koutecký, J.; Michl, J. Neutral and Charged Biradicals, Zwitterions, Funnels in S_1, and Proton Translocation: Their Role in Photochemistry, Photophysics, and Vision. *Angew. Chem., Int. Ed. Engl.* **1987**, *26*, 170−189.
(15) Filatov, M. Assessment of Density Functional Methods for Obtaining Geometries at Conical Intersections in Organic Molecules. *J. Chem. Theory Comput.* **2013**, *9*, 4526−4541.
(16) Atchity, G. J.; Xantheas, S. S.; Ruedenberg, K. Potential Energy Surfaces near Intersections. *J. Chem. Phys.* **1991**, *95*, 1862−1876.
(17) Kazaryan, A.; Kistemaker, J. C. M.; Schäfer, L. V.; Browne, W. R.; Feringa, B. L.; Filatov, M. Understanding the Dynamics Behind the Photoisomerization of a Light-Driven Fluorene Molecular Rotary Motor. *J. Phys. Chem. A* **2010**, *114*, 5058−5067.
(18) Kazaryan, A.; Lan, Z.; Schäfer, L. V.; Thiel, W.; Filatov, M. Surface Hopping Excited-State Dynamics Study of the Photoisomerization of a Light-Driven Fluorene Molecular Rotary Motor. *J. Chem. Theory Comput.* **2011**, *7*, 2189−2199.
(19) Conyard, J.; Addison, K.; Heisler, I. A.; Cnossen, A.; Browne, W. R.; Feringa, B. L.; Meech, S. R. Ultrafast Dynamics in the Power Stroke of a Molecular Rotary Motor. *Nat. Chem.* **2012**, *4*, 547−551.
(20) Briand, J.; Bram, O.; Rehault, J.; Léonard, J.; Cannizzo, A.; Chergui, M.; Zanirato, V.; Olivucci, M.; Helbing, J.; Haacke, S. Coherent Ultrafast Torsional Motion and Isomerization of a Biomimetic Dipolar Photoswitch. *Phys. Chem. Chem. Phys.* **2010**, *12*, 3178−3187.
(21) Dunkelberger, A. D.; Kieda, R. D.; Shin, J. Y.; Rossi Paccani, R.; Fusi, S.; Olivucci, M.; Fleming Crim, F. Photoisomerization and Relaxation Dynamics of a Structurally Modified Biomimetic Photoswitch. *J. Phys. Chem. A* **2012**, *116*, 3527−3533.
(22) Léonard, J.; Schapiro, I.; Briand, J.; Fusi, S.; Paccani, R. R.; Olivucci, M.; Haacke, S. Mechanistic Origin of the Vibrational Coherence Accompanying the Photoreaction of Biomimetic Molecular Switches. *Chem. - Eur. J.* **2012**, *18*, 15296−15304.
(23) Filatov, M. Ensemble DFT Approach to Excited States of Strongly Correlated Molecular Systems. In *Density-Functional Methods for Excited States*; Ferré, N., Filatov, M., Huix-Rotllant, M., Eds.; Top. Curr. Chem.; Springer: Heidelberg, 2016; Vol. *368*, pp 97−124.
(24) Filatov, M. Spin-Restricted Ensemble-Referenced Kohn-Sham Method: Basic Principles and Application to Strongly Correlated Ground and Excited States of Molecules. *WIREs Comput. Mol. Sci.* **2015**, *5*, 146−167.
(25) Weber, W.; Thiel, W. Orthogonalization Corrections for Semiempirical Methods. *Theor. Chem. Acc.* **2000**, *103*, 495−506.
(26) Koslowski, A.; Beck, M. E.; Thiel, W. Implementation of a General Multireference Configuration Interaction Procedure with Analytic Gradients in a Semiempirical Context Using the Graphical Unitary Group Approach. *J. Comput. Chem.* **2003**, *24*, 714−726.
(27) Thiel, W. Semiempirical Quantum-Chemical Methods. *WIREs Comput. Mol. Sci.* **2014**, *4*, 145−157.
(28) Tully, J. C. Molecular Dynamics with Electronic Transitions. *J. Chem. Phys.* **1990**, *93*, 1061−1071.
(29) Barbatti, M. Nonadiabatic Dynamics with Trajectory Surface Hopping Method. *WIREs Comput. Mol. Sci.* **2011**, *1*, 620−633.
(30) Fabiano, E.; Thiel, W. Nonradiative Deexcitation Dynamics of 9H-Adenine: An OM2 Surface Hopping Study. *J. Phys. Chem. A* **2008**, *112*, 6859−6863.
(31) Lan, Z.; Fabiano, E.; Thiel, W. Photoinduced Nonadiabatic Dynamics of Pyrimidine Nucleobases: On-the-Fly Surface-Hopping Study with Semiempirical Methods. *J. Phys. Chem. B* **2009**, *113*, 3548−3555.
(32) Weingart, O.; Lan, Z.; Koslowski, A.; Thiel, W. Chiral Pathways and Periodic Decay in cis-Azobenzene Photodynamics. *J. Phys. Chem. Lett.* **2011**, *2*, 1506−1509.
(33) Casida, M. E.; Jamorski, C.; Bohr, F.; Guan, J. G.; Salahub, D. R. Optical Properties from Density-Functional Theory. In *Nonlinear Optical Materials: Theory and Modeling*; Karna, S. P., Yeates, A. T., Eds.; ACS Symposium Series; American Chemical Society: Washington, DC, 1996; Vol. *628*, pp 145−163.
(34) Becke, A. D. Density-Functional Exchange-Energy Approximation with Correct Asymptotic Behavior. *Phys. Rev. A: At., Mol., Opt. Phys.* **1988**, *38*, 3098−3100.
(35) Lee, C.; Yang, W.; Parr, R. G. Development of the Colle-Salvetti Correlation-Energy Formula into a Functional of the Electron Density. *Phys. Rev. B: Condens. Matter Mater. Phys.* **1988**, *37*, 785−789.
(36) Becke, A. D. A New Mixing of Hartree-Fock and Local Density-Functional Theories. *J. Chem. Phys.* **1993**, *98*, 1372−1377.
(37) Krishnan, R.; Binkley, J. S.; Seeger, R.; Pople, J. A. Self-Consistent Molecular Orbital Methods. XX. A Basis Set for Correlated Wave Functions. *J. Chem. Phys.* **1980**, *72*, 650−654.

DOI: 10.1021/acs.jpclett.5b02575
J. Phys. Chem. Lett. 2016, 7, 105−110